Experimental high gradient testing of a 17.1 GHz photonic band-gap accelerator structure

Citation: Munroe, Brian J. et al. "Experimental High Gradient Testing of a 17.1 GHz Photonic Band-Gap Accelerator Structure." Physical Review Accelerators and Beams 19, 3 (March 2016): 031301

As Published: http://dx.doi.org/10.1103/PhysRevAccelBeams.19.031301

Publisher: American Physical Society

Persistent URL: http://hdl.handle.net/1721.1/111569

Version: Author's final manuscript: final author's manuscript post peer review, without publisher's formatting or copy editing

PSFC/JA-15-77

Experimental High Gradient Testing of a 17.1 GHz Photonic Band-gap Accelerator Structure

Brian J. Munroe, JieXi Zhang, Haoran Xu, Michael A. Shapiro,
Richard J. Temkin

December, 2015

Plasma Science and Fusion Center
Massachusetts Institute of Technology
Cambridge MA 02139 USA

This work was supported by the Department of Energy High Energy Physics, under Grant No. DE-SC0010075.

Experimental High Gradient Testing of a 17.1 GHz Photonic Band-gap Accelerator Structure

Brian J. Munroe, JieXi Zhang, Haoran Xu, Michael A. Shapiro, Richard J. Temkin*
Plasma Science and Fusion Center, Massachusetts Institute of Technology, Cambridge, Massachusetts 02139, USA
(Dated: February 17, 2016)

We report the design, fabrication and high gradient testing of a 17.1 GHz Photonic Band Gap (PBG) accelerator structure. Photonic band-gap (PBG) structures are promising candidates for electron accelerators capable of high-gradient operation because they have the inherent damping of high order modes required to avoid beam breakup instabilities. The 17.1 GHz PBG structure tested was a single cell structure composed of a triangular array of round copper rods of radius 1.45 mm spaced by 8.05 mm. The test assembly consisted of the test PBG cell located between conventional (pillbox) input and output cells, with input power of up to 4 MW from a klystron supplied via a TM_{01} mode launcher. Breakdown at high gradient was observed by diagnostics including reflected power, downstream and upstream current monitors and visible light emission. The testing procedure was first benchmarked with a conventional disc-loaded waveguide structure, which reached a gradient of 87 MV/m at a breakdown probability of 1.19×10^{-1} per pulse per meter. The PBG structure was tested with 100 ns pulses at power levels of less than 90 MV/m in order to limit the surface temperature rise to 120 K. The PBG structure reached up to 89 MV/m at a breakdown probability of 1.09×10^{-1} per pulse per meter. These test results show that a PBG structure can simultaneously operate at high gradients and low breakdown probability, while also providing wakefield damping.

I. INTRODUCTION

Photonic band-gap (PBG) structures continue to be a topic of experimental and theoretical interest in accelerator structure design. PBG accelerator research is conducted at microwave and optical wavelengths and in room temperature and superconducting structures [1–10]. Photonic crystals use a lattice of metallic or dielectric rods to prevent propagation of electromagnetic waves through the lattice at certain frequencies that fall into the band gap [11, 12]. In accelerator applications this allows for a drive mode to be confined by a defect region within the lattice while damping modes at both higher and lower frequencies. A metallic PBG lattice can be designed such that the lowest frequency mode supported by the cavity is the drive mode and all higher order modes (HOMs) are damped. The initial design of a PBG accelerator structure was based on a square lattice as proposed in [13]. A triangular lattice provides better symmetry for accelerator structures, and good agreement with simulation has been shown for a triangular lattice in an accelerator application [14]. A 17.1 GHz, six-cell traveling wave PBG structure based on this triangular lattice was built [15] and tested at MIT, demonstrating acceleration [1]. PBG HOMs have been simulated and the wakefields have been measured [10, 16, 17]. Wakefield damping has been studied in simulation in [18], and optimized wakefield damping via lattice perturbations has been studied in [19]. High-gradient testing of two standing wave PBG structures at 11.4 GHz at SLAC [9, 20] has shown that PBG structures are capable of achieving both low breakdown probability and high-gradient operation. The test at SLAC included a PBG structure with round rods (PBG-R) [9] and an improved structure with elliptical rods (PBG-E) to reduce the temperature rise at the rod surface [20].

Following the successful demonstration of high-gradient operation of a PBG structure at 11.4 GHz at SLAC, both a PBG structure (MIT-PBG) and a reference disc-loaded waveguide (DLWG) structure (MIT-DLWG) were designed and tested at 17.1 GHz at MIT. This paper reports the experimental test results. These structures follow the general design used extensively in previous SLAC single-cell standing wave structure testing [21–29]. The structures are designed with a matching cell on either side of a single high-gradient test cell; only this central cell varies between the two structures. The structure is designed to have the highest electric and magnetic fields in the test cell and significantly reduced fields in the matching cells. The matching cells in both structures have solid cylindrical walls. The structure is axially powered via a reusable TM_{01} mode launcher built at SLAC and scaled from their design [30]. A model of the PBG structure tested at MIT is shown in Fig. 1; the DLWG structure differs only in the center cell pieces. The detailed design of the structures is described in Section II

II. ACCELERATOR TEST STRUCTURE DESIGN

Our design and test strategy follows the techniques pioneered at SLAC. We employ single-high-gradient, standing-wave structures powered using a reusable TM_{01} mode launcher. The SLAC-type mode launchers are

*temkin@mit.edu

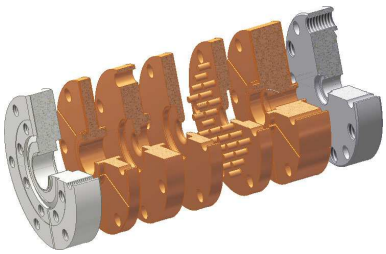

FIG. 1: Expanded three quarter section view of the solid model of the 17.1 GHz PBG structure, showing two coupling cells and central PBG cell. The clamping rods are not shown for clarity. Power is coupled in from a TM_{01} mode launcher (not shown) connected at the left.

driven by an incident TE_{10} mode in rectangular waveguide, WR-62 for the 17.1 GHz launcher, which is then converted to the TM_{01} mode in cylindrical waveguide with a diameter of 0.600 inches.

This cylindrical input waveguide is coupled into a three-cell structure through a coupling iris. The high-gradient center cell is designed to have twice the axial electric field amplitude of the coupling cells on either side, in order to limit breakdowns to the high-gradient cell under test. For the structures described here the aperture for the high-gradient irises relative to wavelength, a/λ, and the thickness of the irises relative to the wavelength, t/λ, were kept the same as the structures tested at 11.4 GHz at SLAC [20]; this makes the center cell and irises effectively part of a periodic accelerator structure of the desired geometry. The two coupling cells and the input coupling iris can be used to tune the frequency and coupling of the structure under test.

While the breakdown structures tested at SLAC were fully brazed, the PBG and DLWG structures tested at MIT and described here were assembled using clamping rods. Our first test structures were fully brazed. They suffered from the difficulty in tuning and in achieving a high quality braze of all of the joints. A clamped structure also allows for the possibility of replacing damaged parts as well as disassembly and reassembly of structures during testing to examine surfaces for damage. The use of a clamped structure is also greatly simplified because of the external vacuum chamber at the MIT standing-wave test stand.

The PBG test structure itself is still fully brazed. This allows better alignment of the two high-gradient irises and guarantees good electrical contact for all of the rods. Brazing the PBG cell also allows the outer wall of the cell to be opened. This allows for the higher-order modes to be radiatively damped in the central cell, which in turn requires an additional layer of rods in the PBG cell. The use of overlapping concentric alignment surfaces between the rest of the cups and the single mating surface at those junctions makes clamping a good alternative for the rest of the structure joints. The fields at these clamped surfaces should be very low and should not cause arcing or breakdown. The positive results observed using a clamped structure are consistent with the results previously observed in clamped structure testing [31, 32].

TABLE I: Common fixed parameters for 17.1 GHz standing-wave structure. Final design values for parameters shown in Fig. 2.

Fixed Parameters	
Rpipe	2.0 mm
Rb	0.25 mm
t	3.07mm
e_r	2.27 mm
D	8.75 mm
a	3.77 mm
a_pipe	4.23 mm
b_conv	7.62 mm

A. Structure Tuning

In addition to the iris geometry, various other structure parameters are fixed by the frequency of the experiment and the geometry of the TM_{01} mode launchers. The diameter of the input waveguide is fixed to that of the mode launcher being used. The diameter of the output waveguide is chosen such that the accelerator mode is below cutoff, thereby reflecting the mode and forming a standing wave structure. The lengths of the cells are fixed by matching the frequency of the π mode to the frequency of the klystron used for testing, and the radii of curvature in the cells are fixed for ease of fabrication. These parameters are shown in an axisymmetric view in Fig. 2 and their values are given in Table I.

When designing the structure the frequency of the π mode and the 1:2:1 field amplitude ratio (from the input cell to the test cell to the output cell) profile are dominated by three tuning parameters: the radius of each of two coupling cells and the aperture of the coupling iris. These tuning parameters of the structure are shown in Fig. 3. The radii of the input and output coupling cells, b_cpl and b_end respectively, are varied in HFSS simulations to find a field profile on axis with approximately half of the peak field amplitude in the coupling cells relative to the central PBG cell. The aperture of the coupling iris, a_cpl, is chosen to achieve critical coupling in the HFSS simulation. Varying a_cpl affects the frequency of the structure so an iterative process of tuning the frequency with the cell radii then adjusting the coupling with the iris aperture must be used to keep the resonant frequency of the entire structure as close as possible to the resonant frequency of the PBG lattice, which is tuned to the center frequency (17.14 GHz) of the klystron.

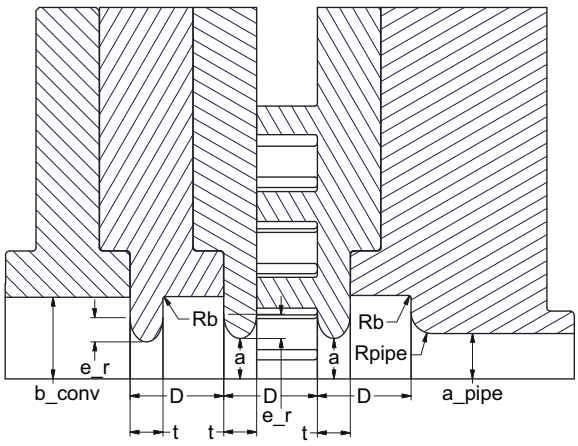

FIG. 2: Axisymmetric views of the assembly drawing of the 17.1 GHz PBG structure showing the fixed parameters of the structures. The five plates that are defined in the drawing correspond to the five copper-colored elements shown in Fig. 1.

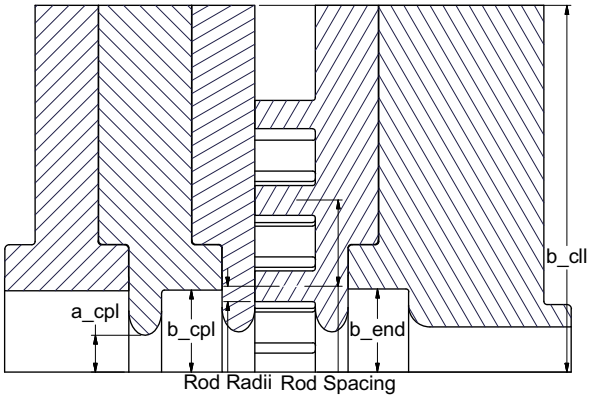

FIG. 3: Axisymmetric views of the assembly drawing of the 17.1 GHz PBG structure showing the tuning parameters for the structure.

B. Design of the Photonic Band-Gap Structure

The photonic band-gap structure for testing at 17.1 GHz is designed as a scaled version of the PBG-R structure described in [20], i.e. the lattice uses only round rods and has a filling factor of $\alpha/\beta = 0.18$. The radius to the outer wall of the PBG cell, b_cll, is chosen to allow the clamping rods for the structure to be placed in the holes in a standard 2.75 inch ConFlat flange. The structure was tuned as described in Sec. II A, and the final design values for the tuning parameters are given in Table II.

The assembly drawings in Figures 2 and 3 also show the major modification to the PBG design for testing at MIT: the open outer wall. Removing the outer wall of the structure provides line-of-sight access to the high-gradient surfaces of the structure, such as the irises and rod faces. Although direct observation of these surfaces in-situ is difficult, the general access to the high-gradient region of the structure allows for optical detection of light produced by breakdowns, with the possibility of localization of the source of this light to identify breakdown location; this will be discussed in more detail in Sec. III C.

TABLE II: Tuning parameters for the 17.1 GHz PBG structure. Final design values for Fig. 3.

Tuning Parameters	
a_cpl	3.45 mm
b_cpl	7.69 mm
b_cll	69.34 mm
b_end	7.78 mm
Rod Radii (α)	1.45 mm
Rod Spacing (β)	8.05 mm

The outer wall in the PBG-E structure previously tested at 11.4 GHz at SLAC does also increase the diffractive quality factor of that structure. To account for this decrease in diffractive Q when moving to an open-walled structure in the 17.1 GHz tests, the number of layers of rods in the 17.1 GHz PBG structure was increased from two in the 11.4 GHz structure to three in the 17.1 GHz structure. The open wall, like in the traveling-wave structure previously tested at MIT, also allows the HOMs to be radiatively damped. While no HOMs should be excited by the TM_{01} mode launcher, testing the open structure validates that a PBG structure with actual damping can operate at high gradients; in contrast any HOMs excited in the SLAC structures would be reflected back into the lattice by the solid wall.

The key results of the PBG structure design are summarized in Figures 4 and 5, showing the magnitude of the reflection from the cavity as a function of frequency and the normalized axial field profile of the structure, respectively. Figure 4 shows the minimum in reflection for the π mode of the structure of -38 dB, which is achieved at 17.137 GHz; this is comfortably within the operating bandwidth of the MIT klystron. Figure 5 shows the desired 1:2:1 pattern in the axial field amplitude, where the central PBG test cell has about twice the field amplitude of the coupling cells on each side.

Field plots for the final design are shown in Fig. 6 and Fig. 7 in a cutaway view through an inner rod and top-down view, respectively. In the cutaway view the 1:2:1 relationship in electric field value can be seen, as well as the increase in surface electric field on the irises. This view also shows the localization of the magnetic field to the defect-facing side of the inner rods. The top-down view shows the uniformity of the accelerating field in the defect region, and the distribution of the magnetic field across the defect-facing side of the inner rod.

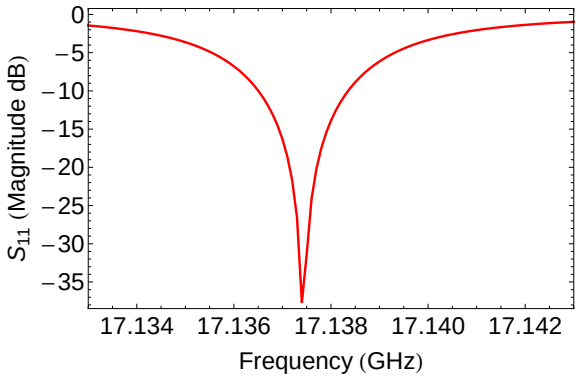

FIG. 4: Calculated reflection as a function of frequency for the 17.1 GHz PBG structure.

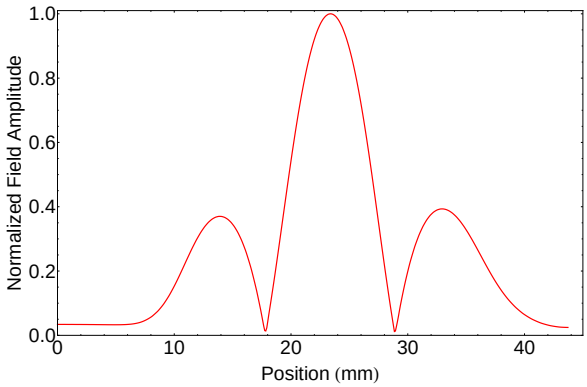

FIG. 5: Normalized profile of simulated electric field on axis in PBG structure; the field amplitude in each coupling cell is approximately half that in the PBG cell.

C. Design of the Disc-Loaded Waveguide Structure

In order to facilitate rapid testing of the disc-loaded waveguide (DLWG) structure for comparison to the 17.1 GHz PBG structure, the DLWG structure was designed with identical parameters wherever possible. This allows for reuse of parts from the PBG structure in the DLWG structure. This means that for the DLWG structure the only tuning parameter was the radius of the high-gradient cell, b_cll. While this means that the coupling to and axial field profile of the final design are not optimized, sufficient coupling at a frequency within the bandwidth of the klystron was found at b_cll = 7.58 mm. The additional fixed parameters determined by the PBG design are shown in Fig. 8 in black, and the tuning parameter b_cll is shown in blue. The coupling is shown in Fig. 9, showing that the π mode has a minimum reflection from the structure occurring at 17.149 GHz with a minimum value of -25 dB.

The axial field profile along the structure is shown in Fig. 10. As in the case of the PBG structure design, an approximately 1:2:1 ratio in field amplitude is calculated. Field plots for the final design are shown in Fig. 11 and Fig. 12 in a cutaway view and top-down view, respectively. In the cutaway view the 1:2:1 relationship in electric field value can be seen, as well as the increase in surface electric field on the irises. This view also shows the localization of the magnetic field to the outer wall of the central cell. The top-down view shows the uniformity of the accelerating field in the central cell, and the

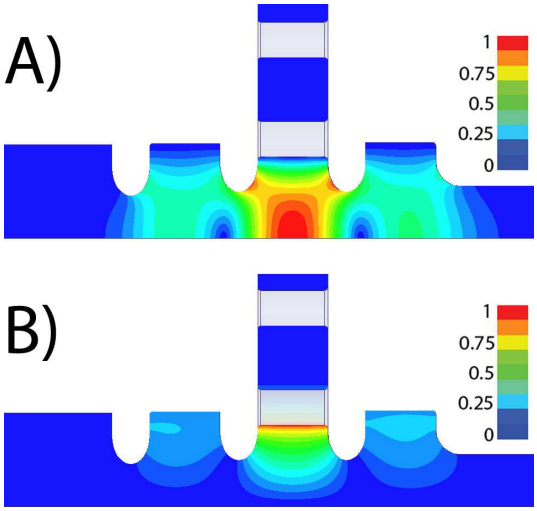

FIG. 6: Electric (A) and magnetic (B) field amplitudes looking at a radial cut of the structure through an inner rod. At an accelerating gradient of 100 MV/m the peak surface electric field amplitude is 200 MV/m at the iris surfaces, and the required input power is 2.4 MW. At the same gradient the peak surface magnetic field occurs on the inner surface of the inner rod, and reaches a value of 900 kA/m. The radial extent of the structure has been cropped for compactness.

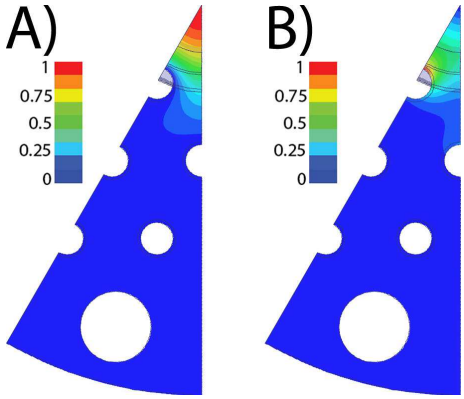

FIG. 7: Electric (A) and magnetic (B) field amplitudes looking at top-down view of a 30 degree section of the structure. The peak surface electric field of 200 MV/m for a 100 MV/m accelerating gradient from 2.4 MW of input power is seen on-axis. The peak surface magnetic field of 900 kA/m for an accelerating gradient of 100 MV/m is confined to the center of the inner surface of the innermost rod. The additional large white space at the bottom of the images is the clamping rod that hold the structure together.

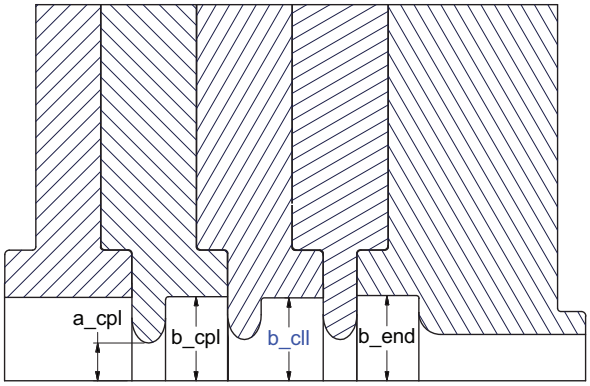

FIG. 8: Axisymmetric views of the assembly drawing of the 17.1 GHz MIT-DLWG structure showing the additional fixed parameters for the structure in black and the one tuning parameter in blue.

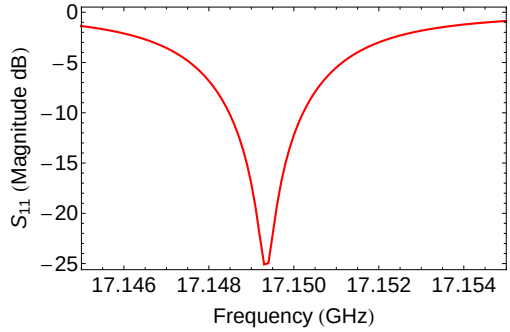

FIG. 9: Calculated reflection as a function of frequency for the 17.1 GHz clamped DLWG structure.

distribution of the magnetic field across the outer wall of the structure.

D. Structure Modeling for Data Analysis

The data collected during experimental operation is in the form of number of breakdowns per unit time versus power incident on the structure. In order to translate this data into breakdown probabilities as a function of field parameters, such as gradient or peak surface temperature rise, calibrations between input power and field must be made. This can be done as described in [20], combining both eigenmode and driven modal HFSS [33] simulations with a resonator response model in Mathematica [34]. This results in a model of the evolution in time of the fields in the structure, from which the various pertinent physical quantities can be calculated.

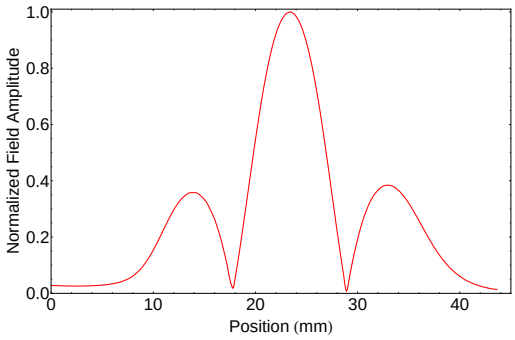

FIG. 10: Normalized electric field profile on axis in DLWG structure; the field amplitude in each coupling cell is approximately half that in the central cell.

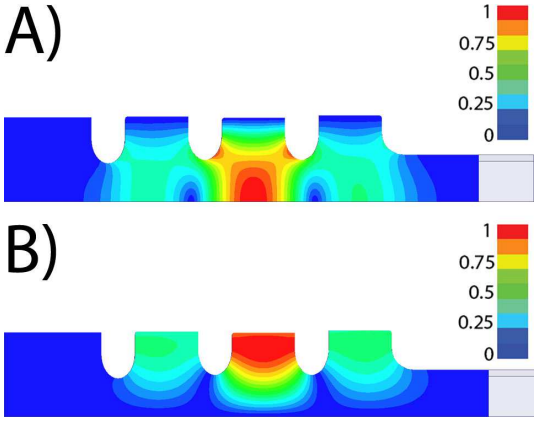

FIG. 11: Electric (A) and magnetic (B) field amplitudes looking at a radial cut of the structure. At an accelerating gradient of 100 MV/m the peak surface electric field amplitude is 197 MV/m at the iris surfaces, and the required input power is 2.0 MW. At the same gradient the peak surface magnetic field occurs along the outer wall of the structure, and reaches a value of 421 kA/m.

III. EXPERIMENTAL SETUP

A. Cold Test

Initial setup and tuning of the clamped PBG and DLWG structures was completed using a vector network analyzer (VNA) and an additional TM_{01} mode launcher. The VNA was connected to the rectangular input of the mode launcher and a measurement of the complex reflection (S_{11}) from the single-port structure is made. This measurement can be used to determine if any tuning of the structure is necessary.

In additional to the S_{11} measurement, the axial field profile in each structure is measured. This is done using the same non-resonant technique described in [20] where a dielectric bead is suspended on a thin dielectric wire along the axis of the structure. The wire used is Ashaway 10/0 black monofilament micro suture thread

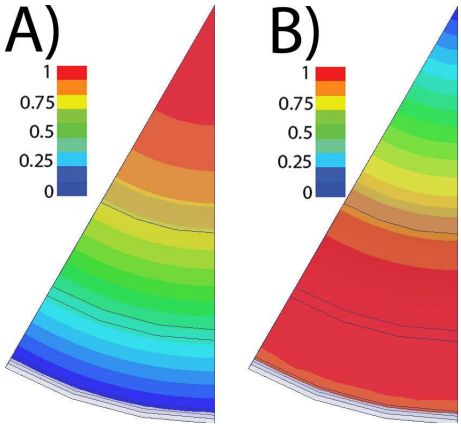

FIG. 12: Electric (A) and magnetic (B) field amplitudes looking at top-down view of a 30 degree section of the structure. The peak surface electric field of 197 MV/m for a 100 MV/m accelerating gradient from 2.0 MW of input power is seen on-axis. The peak surface magnetic field of 421 kA/m for an accelerating gradient of 100 MV/m is on the end plate of the structure.

and the bead is a small drop of super glue. The bead is moved through the structure with the use of a precision translation stage. The structure is suspended with the axis vertical and tension is maintained on the line using lead weights; the translation stage moves perpendicular to the structure axis over a pulley to reduce bouncing of the bead during testing. This field profile is used both to confirm that the structure is operating in the desired π mode and to determine which coupling cell needs to be modified to tune the frequency of the structure.

B. High-Power Testing

Both structures were tested at the MIT Plasma Science and Fusion Center, using a 17.1 GHz traveling-wave relativistic klystron (TWRK) built by Haimson Research Corporation [35]. The rf is generated by a continuous wave rf synthesizer and is gated by a pin diode before entering a solid state rf amplifier chain to drive the klystron, producing up to 25 MW of rf power at a gain of 76 dB. The klystron produces square pulses with pulse lengths between 10 ns and 1000 ns.

The standing-wave structure test stand is isolated from the klystron using a 4.4 dB hybrid to prevent power reflected from the structure during breakdowns from returning to the klystron. This test stand is also vacuum isolated from the klystron with an rf window; this window is limited to a peak power of approximately 10 MW, resulting in a maximum power to the test stand of approximately 4 MW.

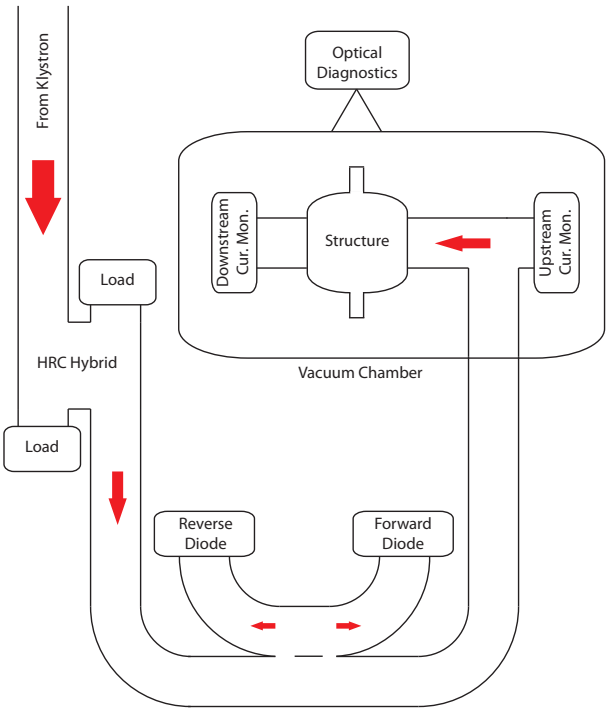

FIG. 13: A schematic view of the MIT standing-wave test stand and associated diagnostics is shown. Power is coupled from the klystron through a 4.4 dB hybrid made by Haimson Research Corporation (HRC) before coupling into the structure. Incident and reflect rf power signals are measured using diode detectors on a 65 dB waveguide directional coupler. Upstream and downstream current monitors are present within the vacuum chamber.

C. Diagnostics

The standing-wave test stand at MIT is setup to include equivalent diagnostics to those available at SLAC. These diagnostics are a measurement of incident and reflected rf power, and upstream and downstream current monitors. In contrast to the SLAC setup, the diagnostics at MIT do not serve a dual purpose of also controlling autonomous operation of the test stand; this simplifies the diagnostic requirements. A schematic view of the standing wave test stand and associated diagnostics is shown in Fig. 13.

The incident and reflected rf power signals are detected using Hewlett Packard HP 8473B low-barrier Schottky diodes. Both signals are detected using the forward and reverse arms of a single high-directivity waveguide directional coupler with 65 dB of attenuation in the measurement arms. The diode traces are recorded by the associated computer system and saved for later analysis. Control of the rf power level and frequency is achieved via manual control of the rf source.

The upstream and downstream current monitors are both composed of copper plates isolated from the body of the mode launcher and structure, respectively. These current monitors are grounded to the body of the vacuum

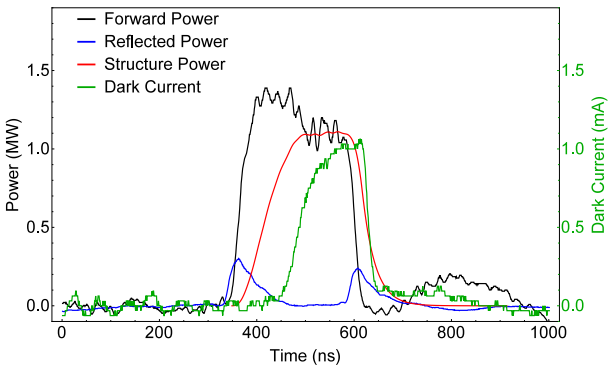

FIG. 14: Sample forward power, black, reflected power, blue, downstream current monitor, green, and calculated structure power, red, traces are shown. This trace was recorded during operation of the pre-test structure, and represents a gradient of 67 MV/m in the PBG structure.

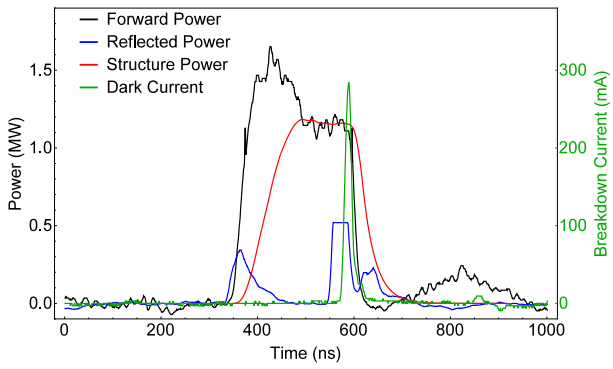

FIG. 15: Sample forward power, black, reflected power, blue, downstream current monitor, green, and calculated structure power, red, traces for a pulse during which a breakdown occurred are shown. This trace was recorded during operation of the pre-test structure, and represents a gradient of 69 MV/m in the PBG structure.

chamber and terminated into 50 Ohm loads on the same LeCroy LT264M oscilloscope used for rf detection. This allows for very good relative timing of different breakdown events compared to the rf pulse. The current monitor signals are used both to monitor the dark current during normal operation and to detect breakdown events. Breakdowns are detected as a binary signal; if the current monitor signal goes off-scale, then a breakdown is determined to have occurred.

Because of the open nature of the clamped 17.1 GHz PBG structure, optical diagnostics are also available at the MIT test stand. During the initial PBG structure testing a video camera was used to visually observe the locations of breakdown during testing. Bright flashes can be seen during breakdown events, and the location of the brightest part of the flash is assumed to correspond to the initiation site of the breakdown.

D. Sample Traces

Data were recorded from the LeCroy LT264M oscilloscope using a LabView routine that records the forward rf signal, reflected rf signal, and downstream current monitor signal for every pulse. A sample set of these traces, as well as the calculated power coupled into the structure corresponding to this forward power pulse, are shown in Fig. 14. The forward power and current monitor traces from each pulse must be analyzed to calculate the power coupled into the structure and whether or not a breakdown occurred. A sample of traces for a pulse during which a breakdown did occur is shown in Fig. 15. The breakdown can be seen as an increase in both the current monitor signal and the reflected power signal to the limit of the oscilloscope range. Note also that the current monitor signal in this figure is on a much larger scale, hundreds of milliamps versus milliamps.

E. Pre-Test Structure

Prior to testing of the final PBG and DLWG structures, a preliminary structure was tested to validate the experimental setup and fabrication techniques. This pre-test structure featured the same design as the PBG structure, including a brazed central PBG cell. Numerous minor issues were identified during this initial testing; they are reported elsewhere [36]

The pre-test structure did identify an important modification of the testing protocol. During operation of the PBG pre-test structure it was found that if breakdowns occurred on a sufficient number of consecutive rf pulses, stable operation could not be re-established without a significant decrease in forward power. Subsequent to one of these "breakdown chains" further breakdowns would be observed below the previous stable operating condition. This behavior significantly delayed efforts to condition the pre-test structure to validate full-power operation of the test stand, and it was determined that in future testing the maximum number of consecutive breakdowns should be limited to prevent setbacks in conditioning of the structures.

IV. DLWG RESULTS

Because of the large body of information about breakdown in disc-loaded waveguide structures, we tested the 17.1 GHz DLWG structure before the PBG structure.

A. Cold Test

The measured resonant frequency and quality factors for the π mode in the 17.1 GHz clamped DLWG structure are shown in Table III; the total or loaded Q, Q_L, is

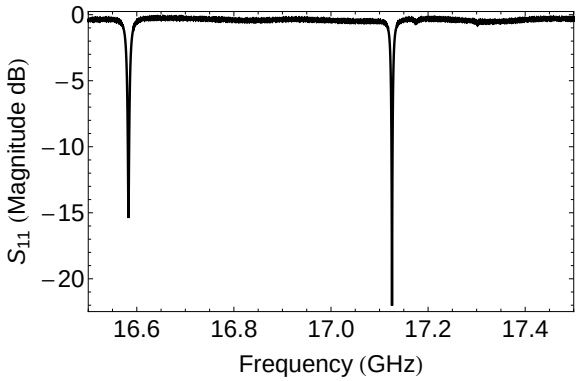

FIG. 16: S_{11} of DLWG structure showing resonances for the $\pi/2$ and π modes at increasing frequency.

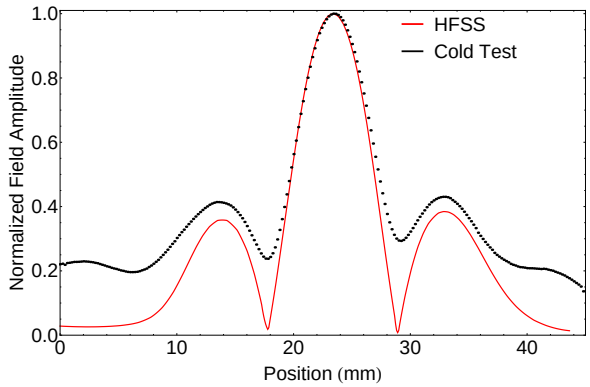

FIG. 17: Comparison of the simulated and measured axial field profiles for the π mode of the DLWG structure.

TABLE III: Q values for the π mode of the DLWG structure. Note that this frequency is measured in air. The operational value is 5 MHz higher in frequency.

Mode	Frequency	Q		
	(GHz)	Q_0	Q_{ext}	Q_L
π	17.126	5170	5270	2610

determined from the measured ohmic Q, Q_0, and the diffractive or external Q, Q_{ext}, as $Q_L^{-1} = Q_0^{-1} + Q_{ext}^{-1}$. The measured reflection data from which these values are obtained are shown in Fig. 16. The observed frequency of the DLWG structure is approximately 20 MHz below the design value. The expected shift in frequency resulting from measuring the reflection in air instead of vacuum is 5 MHz. The remaining 15 MHz shift in frequency is likely due to small fabrication errors across all of the pieces of the clamped assembly. The use of simple, low-torque clamping may have also played a role in detuning the structure, as well as causing some of the mismatch between the simulated and measured fields. The DLWG structure was tuned by shortening the central cell so that the coupling cells could be used for testing of additional PBG cavities.

A comparison of the measured axial field profile to the simulation results for the DLWG structure is shown in Fig. 17. This confirms that the structure is operating in the π mode at the desired resonant frequency, with approximately a 1:2:1 ratio of field amplitude across the three cells. Given that the coupling to the structure is very close to critical, the non-zero field amplitude seen outside of the coupling cells is likely a result of noise in the measurement. This can result from larger step sizes in the bead position, contamination of super glue on the thread suspending the bead, a super glue bead that is too small, or disturbances to the setup during measurement.

B. Testing Methodology

Based on our experience with the pre-test structure, the number of consecutive breakdowns in the DLWG structure was limited to 10 for the duration of testing, with a target of not more than 5 consecutive breakdowns. Because the surface magnetic fields in the DLWG structure are so much lower, there is no concern about pulsed heating in testing this structure.

The DLWG structure began testing at a flat-top pulse length of 100 ns. This was to limit the pulse energy at high gradients in an effort to minimize consecutive breakdowns. The power in the structure was increased slowly, keeping the steady state breakdown rate on the order of ten per hour, with the final objective of reaching a maximum gradient of at least 90 MV/m.

C. Results

Testing of the DLWG structure also proceeded in multiple phases. Phase 1 of testing began with the initial conditioning of the structure at a flat-top pulse length of 70 ns. This pulse length was increased to the desired 100 ns flat top after the initial day of conditioning, and the power level in the structure was increased as-tolerated by the limitation on number of breakdowns per hour. The structure reached a gradient of approximately 65 MV/m at a pulse length of 100 ns before breakdowns at the structure-launcher joint were detected. Due to the setup of the structure test stand, this joint, which has to be made in-situ and requires precise alignment of a shim as well as even torque on all of the bolts, was physically difficult to access and so subject to misalignment.

After the poor joint between the structure and launcher was detected, the structure was removed and reinstalled with extra care to ensure that the shim was properly positioned and that the bolts were torqued evenly. The structure was quickly reconditioned to 65 MV/m at the beginning of Phase 2 of testing, and no

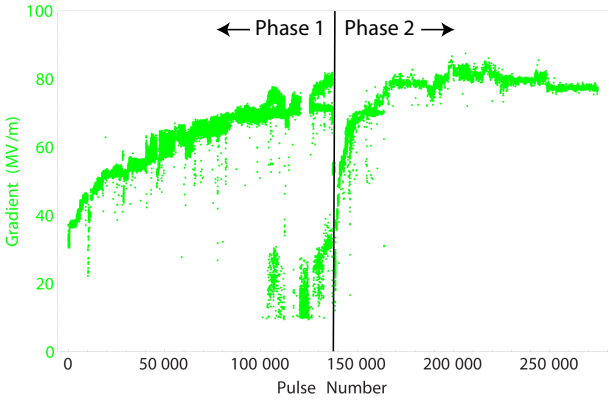

FIG. 18: Summarized results showing the gradient for the duration of DLWG structure testing at MIT. The two phases of testing are separated by a vertical black line, with Phase 1 comprising all of the data to the left of the line, and Phase 2 comprising all of the data shown to the right of the line.

subsequent problems with the joint were observed. The structure was then processed at large breakdown probabilities up to a maximum gradient of 90 MV/m at a pulse length of 100 ns, a breakdown probability of 1.2×10^{-1} per pulse per meter of structure, and an input power of 1.6 MW. Processing was observed, as both the dark current from the structure measured by the downstream current monitor and the breakdown probability at constant power levels decreased. Note that the upstream current monitor (not recorded) showed zero dark current for the majority of testing, but did show current during breakdown events. Above 85 MV/m a small upstream dark current signal, two orders of magnitude smaller than the downstream signal, was observed. When gradient was increased above 90 MV/m, periods of stable operation were observed before reaching a threshold-like behavior. This does not appear to be a true threshold, as continued operation at a pulse length of 100 ns at a gradient of 90 MV/m increased the duration of these stable periods of operation at greater than 90 MV/m. The structure may be capable of reaching higher gradients with continued processing. The analyzed gradient versus total pulse number for the combined testing of the MIT DLWG structure is shown in Fig. 18, showing the increase in gradient with processing. In total Phase 1 comprised approximately 140,000 pulses. The rapid return to previous operating levels at the start of Phase 2 can be seen from 140,000 to 150,000 pulses into testing. Phase 2 continued for a total of 160,000 pulses, making the total number of pulses seen by the DLWG structure approximately 300,000.

D. Phase 1

The structure processed readily to a gradient of 65 MV/m at a breakdown probability of 0.63 per pulse per meter for a pulse length of 100 ns. At gradients higher than this small signals on the upstream current monitor, which typically read no dark current signal during non-breakdown operation, were observed just before the end of the rf pulse. These small upstream current monitor signals were an order of magnitude or more below typical breakdown signals. Correlated with these signals were increases in the power reflected by the structure. This behavior is indicative of arcing or breakdowns at the structure-launcher joint; operating the structure off-resonance found that breakdowns were still occurring, confirming that the joint was contributing to the breakdown rate. The structure had previously been tested off-resonance at low power levels and no breakdowns were observed, indicating that breakdowns at the joint between the structure and launcher only began affecting performance at gradients above 60-65 MV/m for 100 ns pulses.

After the joint was confirmed to be affecting performance, the structure was removed, the reflection was remeasured, and the structure was reinstalled to begin Phase 2 of testing.

E. Phase 2

During Phase 2 of testing the structure was quickly returned to a gradient of 65 MV/m with only a minimal amount of processing. The power level in the structure was then increased as-tolerated by a maximum breakdown rate of 50 or more per hour during operation at 1 Hz. Although this rate is higher than the desired maximum steady-state breakdown rate, the structure was consistently in a transient condition where a higher breakdown rate can be tolerated. This transient condition was identified by both the instantaneous change in breakdown rate, i.e. time between breakdowns was generally increasing, and the decrease in dark current. The dark current was observed to increase significantly with small increases in input power, but would then decrease as the structure was operated at the same input power level. The increase in gradient at the same relatively large breakdown probability can be seen in Fig. 19, where the data from Phase 1 and 2 are combined to a single data set and are shown in purple. Note that this data is combined because the structure is still operating in an un-processed state during both phases, as opposed to measuring a fully- or partially-processed breakdown probability after a maximum gradient has been reached.

This processing was continued to a maximum gradient of 87 MV/m at a pulse length of 100 ns. The dark current as a function of gradient for part of this processing is shown in Fig. 20. The data shows a consistent increase in dark current with gradient, as expected for dark current resulting from field emission. At each increase in gradient the dark current starts out at a higher value before stabilizing. This is indicative of the surface improving with processing. This can be seen more clearly in Fig. 21, which shows the same data set plotted as a function of the pulse number. This is a representative sampling of

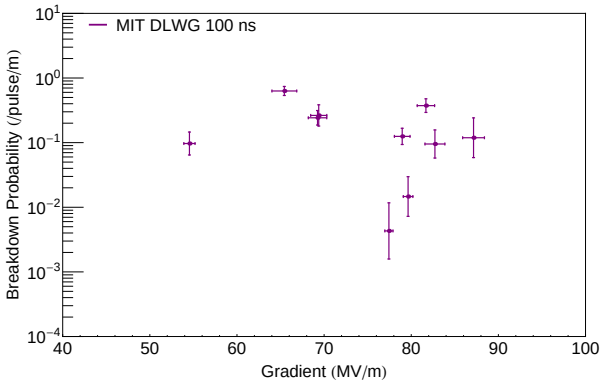

FIG. 19: Breakdown probability as a function of gradient for the DLWG structure.

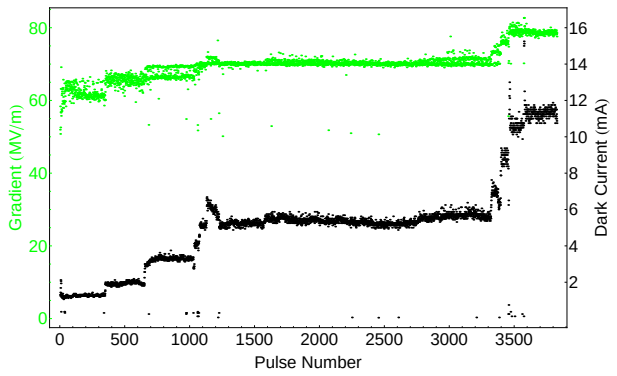

FIG. 21: Dark current in mA and gradient in MV/m as a function of pulse number for a representative sampling from one day of testing of DLWG structure.

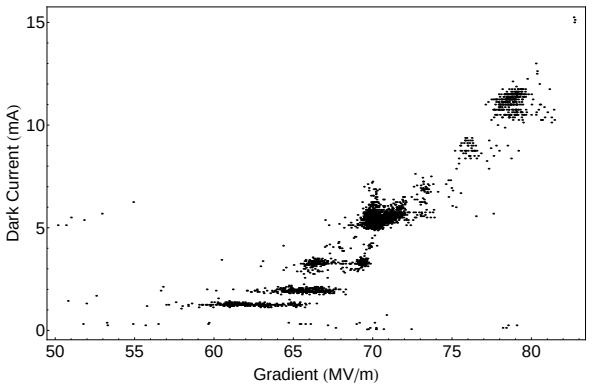

FIG. 20: Dark current in mA as a function of gradient in MV/m for one day of testing of MIT-DLWG structure. A representative sampling of the data is shown.

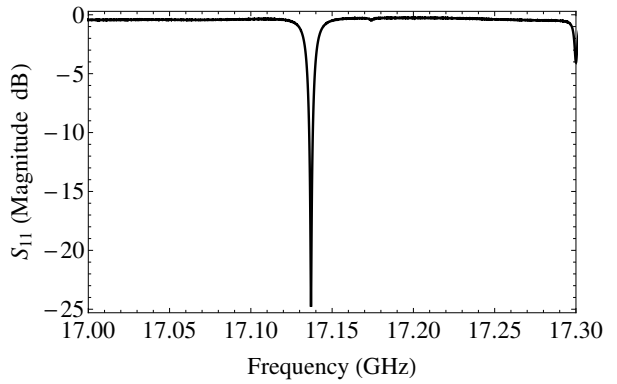

FIG. 22: S_{11} of the PBG structure showing resonance for the π mode.

the data; the structure saw approximately 40,000 pulses on this day.

This trend of increasing length of stable operation suggests that continued operation of the structure at or near 90 MV/m will result in processing and allow the gradient to be further increased. Continued operation at 87 MV/m should also decrease the breakdown probability and dark current at that gradient as the structure processes. Evidence of this processing can be seen in the multiple data points around 80 MV/m with a decreasing breakdown probability, as well as the data points at approximately constant breakdown probability and increasing gradient, as shown on Fig. 19. Testing of the DLWG structure up to a gradient of 90 MV/m was considered adequate since the PBG structure testing was not designed to exceed that gradient. Therefore, the DLWG structure testing was halted and the PBG structure was installed.

V. PBG RESULTS

A. Cold Test

Following testing of the DLWG reference structure the PBG structure (MIT-PBG) was tested. This structure reused all of the components used in the DLWG structure except the cylindrical central cell. The measured reflection of the structure for the PBG structure is shown in Fig. 22. The frequency for this structure is a good match to the design value of 17.137 GHz. The data in Fig. 22 is restricted to the π mode of the structure, as confirmed by the axial field profile shown in Fig. 23, which compares the measured field profile to the field profile from simulation. There is significant noise in the field profile shown in Fig. 23. This is the result of fraying of the thread used to suspend the dielectric bead used for the measurement. The quality factor and frequency of the operational mode of the clamped PBG structure calculated from the S_{11} are given in Table IV.

TABLE IV: Q values for the π mode of the PBG structure. Note that this frequency is measured in air. The resonant frequency in vacuum is 5 MHz higher.

Mode	Frequency	Q		
	(GHz)	Q_0	Q_{ext}	Q_L
π	17.136	4750	6100	2670

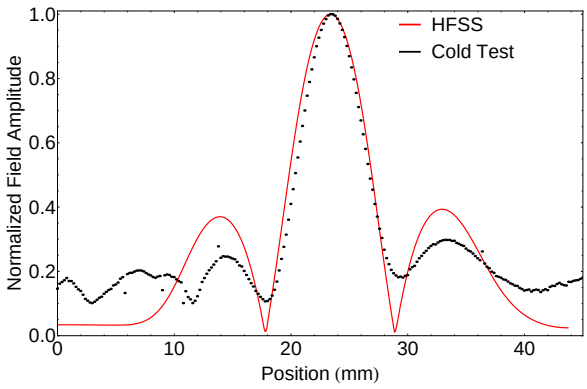

FIG. 23: Comparison of the simulated and measured axial field profiles for the π mode of the PBG structure.

B. Testing Methodology

The testing of the PBG structure followed the same general testing methodology used in the DLWG structure. The number of consecutive breakdowns in the PBG structure was limited to 10 for the duration of testing, with a target of not more than 5 consecutive breakdowns. Because of the high surface magnetic fields present in the PBG structure, the PBG structure was limited to a maximum surface temperature rise of 120 K.

Testing of the PBG structure was conducted entirely at a flat-top pulse length of 100 ns. As in the DLWG structure testing, this serves to limit the pulse energy to avoid consecutive breakdowns. For the PBG structure this shorter pulse length also allows higher gradients to be reached for the same temperature rise. Given this pulse length, and the allowed surface temperature rise, the maximum allowed gradient for the PBG structure is 90 MV/m.

C. Results

Testing of the PBG structure proceeded in a single phase, with no problems at the joint between the structure and mode launcher observed. Processing of the structure proceeded extremely quickly, with the structure ultimately reaching the maximum allowed gradient of 90 MV/m in fewer than 50,000 pulses at an input power of 1.9 MW. This is in contrast to the DLWG structure which took over 300,000 pulses to reach a gradient of 90 MV/m. Very few total breakdowns were observed during this processing, and almost all of those breakdowns occurred in groups of fewer than five events. The gradient, temperature rise, and total number of breakdowns during testing can be seen in Fig. 24. It is expected that, if the temperature limit was relaxed, the structure would achieve higher gradients at the same pulse length without any limiting behavior due to breakdowns.

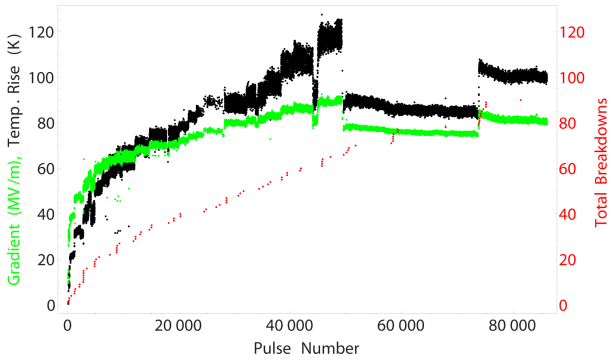

FIG. 24: Summarized results showing the gradient (green), temperature rise (black), and total number of breakdowns (red) for the PBG testing. Note the extremely low breakdown rate even during initial processing.

The PBG structure reached a maximum gradient of 89 MV/m at a pulse length of 100 ns and a breakdown probability of 1.1×10^{-1} per pulse per meter of structure. This breakdown probability was consistent throughout the duration of processing the structure from approximately 65 MV/m to the maximum gradient of 89 MV/m. During processing the power is increased such that the breakdown probability remains relatively constant; if the probability is too high the structure may be damaged and if the probability is too low the structure does not process efficiently. This processing can be seen in Fig. 25 as the series of data points at constant breakdown probability of 1.09×10^{-1} per pulse per meter of structure. The initial processing to 75 MV/m happened very quickly and is not shown on Fig. 25.

Once the maximum gradient was confirmed, the power was reduced to begin collecting statistics to determine the breakdown probability at gradients below the maximum processed value. Because the overall breakdown probability in the PBG-2 structure is low, it is more difficult to obtain a sufficient range of breakdown probabilities without going above the allowed gradient. This necessitates longer periods of operation at a fixed gradient, as seen in Fig. 24 above 50,000 pulses. The minimum breakdown probability was 3.2×10^{-2} per pulse per meter of structure at a gradient of 76 MV/m and a pulse length of 100 ns. This is nearly identical to the breakdown probability of 3.3×10^{-2} per pulse per meter of structure at a gradient of 81 MV/m and a pulse length of 100 ns obtained later in testing. This suggests that the structure has not reached a final steady-state breakdown probability, and more testing is required to determine the final

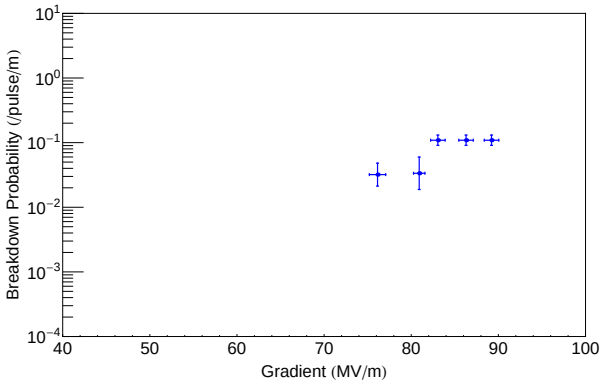

FIG. 25: Breakdown probability as a function of gradient for the PBG structure.

performance of the structure.

One possible explanation for the rapid processing of the PBG structure is the use of the coupling cells from the DLWG structure. These cells were already processed up to a gradient of 90 MV/m during the DLWG testing, and surface changes were evident upon inspection prior to assembly of the PBG structure. This suggests that smoother surface finishes on the coupling cells may reduce processing time in future testing.

D. Post Test

After the conclusion of high-power testing, the PBG structure was removed and the cold test was repeated. This indicated a slight frequency shift of 4 MHz, however the Q_0 of the structure was unchanged within the error of the measurement technique. These results are summarized in Table V. After the cold test the structure was disassembled and examined under an optical microscope. Note that, because of the clamped nature of the structure, this is a non-destructive process, and further testing of the structure is still possible. Optical inspection of the PBG rods showed no indication of pulsed heating damage along the length. There is no obvious difference between either the machined or the brazed ends of the inner-layer rods when compared to the outer-layer rods; the outer-layer rods can be considered unchanged during testing because the field is much lower there. A small amount of pitting indicative of breakdowns was observed on the irises, suggesting that the breakdowns detected during testing occurred at those locations. This conclusion is supported by qualitative visual evidence during testing, where breakdown flashes were observed at the ends of the PBG cell. The combined results of this post test support the conclusion that the PBG structure was undamaged during testing and the observed conditioning of the structure was consistent with conditioning of undamped accelerator structures.

TABLE V: Q values for the π mode of the PBG structure before and after high-power testing. Note that this frequency is measured in air. The operational value is 5 MHz higher in frequency.

Mode	Frequency	Q		
	(GHz)	Q_0	Q_{ext}	Q_L
π before	17.136	4750	6100	2670
π after	17.140	4720	6550	2740

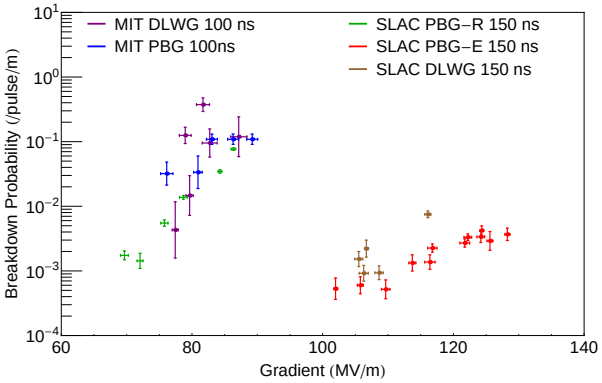

FIG. 26: Breakdown probability as a function of gradient for MIT-PBG, MIT-DLWG, SLAC PBG-R, SLAC PBG-E, and SLAC DLWG structures. For the MIT-DLWG structure only data after the return to high-gradient operation in Phase 2 is shown.

VI. COMPARISON WITH 11.4 GHZ SLAC DATA

Of particular interest in the testing of the PBG structure at MIT is how it performed relative to the similar structures tested at lower frequency, in particular the structures tested at 11.4 GHz in collaboration with SLAC and presented in [9] and [20]. Results from three relevant 11.4 GHz structures are shown here: a DLWG structure (SLAC DLWG), a PBG structure using round rods (SLAC PBG-R), and a PBG structure using elliptical rods for the inner layer and round rods for all other layers (SLAC PBG-E). The breakdown probabilities as functions of gradient for the MIT-DLWG, MIT-PBG, SLAC PBG-R, SLAC PBG-E, and SLAC DLWG structures are shown in Fig. 26. The SLAC data is only shown for a flat-top pulse length of 150 ns, as this is the shortest pulse length tested at SLAC. Because of the change in frequency, however, the number of rf periods, which may be relevant to the breakdown probability, is the same between a 150 ns pulse at 11.4 GHz and a 100 ns pulse at 17.1 GHz.

VII. DISCUSSION AND CONCLUSIONS

It is expected that further testing of the MIT-PBG would continue to show improvements in achievable gra-

dient and breakdown probability, however this processing is expected to proceed slowly because the structure has already reached the maximum input power allowed by the temperature rise limitation. Both the MIT-DLWG structure and the MIT-PBG structure have seen fewer than 10^6 pulses, which is an order of magnitude fewer pulses than in typical testing at SLAC. Breakdowns are assumed to be a necessary step in rf processing, i.e. the structure must see a large number of breakdowns prior to being fully processed. Provided that the hysteresis observed in the test structure at MIT can be avoided, additional breakdowns should continue to process the MIT-DLWG structure.

An alternative to the idea that 10^6 pulses or more are required for conditioning is presented in [37], where conditioning of a 22 cell traveling-wave copper linac is achieved in 1.2×10^5 pulses, and a 22 cell traveling-wave stainless steel-copper hybrid linac is demonstrates significant conditioning after 1.5×10^5 pulses. While these structures were tested using the same klystron and range of repetition rates as the MIT-DLWG and MIT-PBG structures, they are not direct comparisons both because they are traveling-wave structures, and because they were tested as part of a breakdown protection circuit. This circuit limited the amount of rf energy that could be fed into any single breakdown event. This is consistent with the hysteresis observed in the test structure at MIT, suggesting that conditioning is most effective when only a small amount of energy is deposited into any given breakdown event. The initial surface finish of the structures likely also affects the number of pulses required for conditioning, introducing an additional variation between the structures described here and those tested in [37].

Two high gradient standing-wave accelerator structures, one based on a disc-loaded waveguide and one based on a photonic band-gap cavity, have been tested for breakdown performance at MIT and each achieved gradients of at least 90 MV/m at a pulse length of 100 ns and breakdown probability of 1.2×10^{-1} per pulse per meter of structure respectively and 1.1×10^{-1} per pulse per meter of structure respectively. A post test of the PBG structure indicated that it was undamaged during testing. This result shows that PBG accelerator structures can operate at comparable gradients and breakdown probabilities as undamped disc-loaded waveguide structures. Results show that the MIT-PBG structure performed comparably to the SLAC PBG-R structure. Continued testing of the MIT-PBG structure may improve upon this performance. The performance of the MIT-PBG structure is also comparable to the performance of the MIT-DLWG structure, suggesting that PBG structures are viable candidates for future accelerator applications requiring high-gradient, low breakdown probability operation with wakefield damping.

VIII. ACKNOWLEDGMENTS

This work was supported by the Department of Energy High Energy Physics, under Grant No. DE-SC0010075.

The authors would like to thank Dr. Jake Haimson for very valuable discussions and Mr. Ivan Mastovsky for engineering support in operating the accelerator.

[1] E. I. Smirnova, A. S. Kesar, I. Mastovsky, M. A. Shapiro, and R. J. Temkin, Phys. Rev. Lett. **95**, 074801 (2005), URL http://link.aps.org/doi/10.1103/PhysRevLett.95.074801.

[2] E. I. Simakov, S. S. Kurennoy, J. F. O'Hara, E. R. Olivas, and D. Y. Shchegolkov, Phys. Rev. ST Accel. Beams **17**, 022001 (2014), URL http://link.aps.org/doi/10.1103/PhysRevSTAB.17.022001.

[3] E. I. Simakov, S. A. Arsenyev, W. B. Haynes, D. Y. Shchegolkov, N. A. Suvorova, T. Tajima, C. H. Boulware, and T. L. Grimm, Applied Physics Letters **104**, 242603 (2014).

[4] C. A. Bauer, G. R. Werner, and J. R. Cary, Phys. Rev. ST Accel. Beams **17**, 051301 (2014), URL http://link.aps.org/doi/10.1103/PhysRevSTAB.17.051301.

[5] Z. Wu, R. J. England, C.-K. Ng, B. Cowan, C. McGuinness, C. Lee, M. Qi, and S. Tantawi, Phys. Rev. ST Accel. Beams **17**, 081301 (2014), URL http://link.aps.org/doi/10.1103/PhysRevSTAB.17.081301.

[6] C.-K. Ng, R. J. England, L.-Q. Lee, R. Noble, V. Rawat, and J. Spencer, Phys. Rev. ST Accel. Beams **13**, 121301 (2010), URL http://link.aps.org/doi/10.1103/PhysRevSTAB.13.121301.

[7] G. R. Werner, C. A. Bauer, and J. R. Cary, Phys. Rev. ST Accel. Beams **12**, 071301 (2009), URL http://link.aps.org/doi/10.1103/PhysRevSTAB.12.071301.

[8] M. Masullo, A. Andreone, E. Di Gennaro, S. Albanese, F. Francomacaro, M. Panniello, V. Vaccaro, and G. Lamura, Microwave and optical technology letters **48**, 2486 (2006).

[9] R. A. Marsh, M. A. Shapiro, R. J. Temkin, V. A. Dolgashev, L. L. Laurent, J. R. Lewandowski, A. D. Yeremian, and S. G. Tantawi, Phys. Rev. ST Accel. Beams **14**, 021301 (2011), URL http://link.aps.org/doi/10.1103/PhysRevSTAB.14.021301.

[10] C. Jing, F. Gao, S. Antipov, Z. Yusof, M. Conde, J. G. Power, P. Xu, S. Zheng, H. Chen, C. Tang, et al., Phys. Rev. ST Accel. Beams **12**, 121302 (2009), URL http://link.aps.org/doi/10.1103/PhysRevSTAB.12.121302.

[11] E. Yablonovitch, Phys. Rev. Lett. **58**, 2059 (1987), URL http://link.aps.org/doi/10.1103/PhysRevLett.58.2059.

[12] S. John, Phys. Rev. Lett. **58**, 2486 (1987), URL http://link.aps.org/doi/10.1103/PhysRevLett.58.2486.

[13] D. R. Smith, S. Schultz, N. Kroll, M. Sigalas, K. M. Ho, and C. M. Soukoulis, Applied Physics Letters **65**, 645 (1994), URL http://link.aip.org/link/?APL/65/645/1.

[14] M. A. Shapiro, W. J. Brown, I. Mastovsky, J. R. Sirigiri, and R. J. Temkin, Phys. Rev. ST Accel. Beams **4**, 042001 (2001), URL http://link.aps.org/doi/10.1103/PhysRevSTAB.4.042001.

[15] E. I. Smirnova, I. Mastovsky, M. A. Shapiro, R. J. Temkin, L. M. Earley, and R. L. Edwards, Phys. Rev. ST Accel. Beams **8**, 091302 (2005), URL http://link.aps.org/doi/10.1103/PhysRevSTAB.8.091302.

[16] R. A. Marsh, M. Shapiro, R. J. Temkin, and E. I. Smirnova, in *Proceedings of the 2007 Particle Accelerator Conference, Albuquerque, New Mexico* (2007), pp. 3002–3004.

[17] R. A. Marsh, M. A. Shapiro, R. J. Temkin, E. I. Smirnova, and J. F. DeFord, Nuclear Instruments and Methods in Physics Research Section A: Accelerators, Spectrometers, Detectors and Associated Equipment **618**, 16 (2010), ISSN 0168-9002, URL http://www.sciencedirect.com/science/article/pii/S0168900210003670.

[18] M. Hu, B. J. Munroe, M. A. Shapiro, and R. J. Temkin, Phys. Rev. ST Accel. Beams **16**, 022002 (2013), URL http://link.aps.org/doi/10.1103/PhysRevSTAB.16.022002.

[19] E. I. Simakov, W. B. Haynes, S. S. Kurennoy, J. F. O'Hara, E. R. Olivas, and D. Y. Shchegolkov, in *Proceedings of IPAC2012, New Orleans, Louisiana, USA* (2012), pp. 2801–2803.

[20] B. J. Munroe, A. M. Cook, M. A. Shapiro, R. J. Temkin, V. A. Dolgashev, L. L. Laurent, J. R. Lewandowski, A. D. Yeremian, S. G. Tantawi, and R. A. Marsh, Phys. Rev. ST Accel. Beams **16**, 012005 (2013), URL http://link.aps.org/doi/10.1103/PhysRevSTAB.16.012005.

[21] V. Dolgashev, S. Tantawi, C. Nantista, Y. Higashi, and T. Higo, in *Proceedings of the 2004 Linear Accelerator Conference, Lübeck, Germany, 2004* (DESY, Hamburg, 2004), pp. 766–768.

[22] V. Dolgashev, S. Tantawi, C. Nantista, Y. Higashi, and T. Higo, in *Proceedings of the 21st Particle Accelerator Conference, Knoxville, 2005* (IEEE, Piscataway, NJ, 2005), pp. 595–599.

[23] V. Dolgashev, S. Tantawi, C. Nantista, Y. Higashi, and T. Higo, in *Proceedings of the 2007 Particle Accelerator Conference, Albuquerque, New Mexico* (2007), pp. 2430–2432.

[24] V. Dolgashev, S. Tantawi, Y. Higashi, and T. Higo, in *Proceedings of the 11th European Particle Accelerator Conference, Genoa, 2008* (EPS-AG, Genoa, Italy, 2008), pp. 742–744.

[25] V. Dolgashev, AIP Conference Proceedings **1299**, 274 (2010), URL http://link.aip.org/link/?APC/1299/274/1.

[26] V. Dolgashev, S. Tantawi, Y. Higashi, and B. Spataro, in *Proceedings of the 25th International Linear Accelerator Conference LINAC10, Tsukuba, Japan* (2010), pp. 1043–1047.

[27] V. Dolgashev, S. Tantawi, Y. Higashi, and B. Spataro, Applied Physics Letters **97**, 171501 (pages 3) (2010), URL http://link.aip.org/link/?APL/97/171501/1.

[28] V. Dolgashev, Z. Li, S. Tantawi, A. Yeremian, Y. Higashi, and B. Spataro, in *Proceedings of the 2011 International Particle Accelerator Conference, San Sebastian, Spain* (2011), pp. 241–243.

[29] V. Dolgashev, S. Tantawi, A. Yeremian, Y. Higashi, and B. Spataro, in *Proceedings of the 1st International Particle Accelerator Conference: IPAC'10, Kyoto, Japan* (2010).

[30] C. Nantista, S. Tantawi, and V. Dolgashev, Phys. Rev. ST Accel. Beams **7**, 072001 (2004), URL http://link.aps.org/doi/10.1103/PhysRevSTAB.7.072001.

[31] S. Döbert, C. Adolphsen, W. Wuensch, C. Achard, A. Grudiev, S. Heikkinen, I. Syratchev, M. Taborelli, and I. Wilson, Tech. Rep., United States. Department of Energy. Office of Science (2004).

[32] B. Spataro, D. Alesini, V. Chimenti, V. Dolgashev, Y. Higashi, M. Migliorati, A. Mostacci, R. Parodi, S. Tantawi, and A. Yeremian, Nuclear Instruments and Methods in Physics Research Section A: Accelerators, Spectrometers, Detectors and Associated Equipment **657**, 88 (2011).

[33] *High Frequency Structure Simulator, Ansoft Corporation, http://www.hfss.com.*

[34] *Mathematica 8, Wolfram Research, http://www.wolfram.com.*

[35] J. Haimson and B. Mecklenburg, in *AIP CONFERENCE PROCEEDINGS* (IOP INSTITUTE OF PHYSICS PUBLISHING LTD, 2003), pp. 34–45.

[36] B. J. Munroe, Ph.D. thesis, Massachusetts Institute of Technology (2015).

[37] J. Haimson and B. Mecklenburg, in *ADVANCED ACCELERATOR CONCEPTS: Proceedings of the Thirteenth Advanced Accelerator Concepts Workshop* (AIP Publishing, 2009), vol. 1086, pp. 464–469.